JACS
JOURNAL OF THE AMERICAN CHEMICAL SOCIETY

ARTICLE

pubs.acs.org/JACS

Paramagnetic-Based NMR Restraints Lift Residual Dipolar Coupling Degeneracy in Multidomain Detergent-Solubilized Membrane Proteins

Lei Shi,[†] Nathaniel J. Traaseth,[‡] Raffaello Verardi,[‡] Martin Gustavsson,[‡] Jiali Gao,[†] and Gianluigi Veglia*[,†,‡]

[†]Department of Chemistry and [‡]Department of Biochemistry, Molecular Biology, and Biophysics, University of Minnesota, Minneapolis, Minnesota 55455, United States

Supporting Information

ABSTRACT: Residual dipolar couplings (RDCs) are widely used as orientation-dependent NMR restraints to improve the resolution of the NMR conformational ensemble of biomacromolecules and define the relative orientation of multidomain proteins and protein complexes. However, the interpretation of RDCs is complicated by the intrinsic degeneracy of analytical solutions and protein dynamics that lead to ill-defined orientations of the structural domains (ghost orientations). Here, we illustrate how restraints from paramagnetic relaxation enhancement (PRE) experiments lift the orientational ambiguity of multidomain membrane proteins solubilized in detergent micelles. We tested this approach on monomeric phospholamban (PLN), a 52-residue membrane protein, which is composed of two helical domains connected by a flexible loop. We show that the combination of classical solution NMR restraints (NOEs and dihedral angles) with RDC and PRE constraints resolves topological ambiguities, improving the convergence of the PLN structural ensemble and giving the depth of insertion of the protein within the micelle. The combination of RDCs with PREs will be necessary for improving the accuracy and precision of membrane protein conformational ensembles, where three-dimensional structures are dictated by interactions with the membrane-mimicking environment rather than compact tertiary folds common in globular proteins.

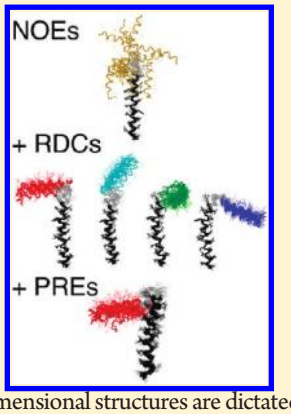

INTRODUCTION

Residual dipolar couplings (RDCs) constitute an excellent source of structural and dynamic information.[1−4] Their use spans from structural refinement[1,5,6] to the characterization of unfolded proteins[7−11] and excited states of biomolecules.[12,13] RDCs are also valuable NMR parameters to determine the relative orientation of multidomain proteins and protein complexes, where interdomain or interprotein nuclear Overhauser effects (NOEs) are scarce.[4,14,15]

However, the inherent degeneracy of RDCs (ghost orientations) complicates the extraction of orientational information.[16] It was originally thought that the RDC equation resulted in 8-fold degeneracy for peptide plane orientations,[16] but recently it was shown that the analytical solution contains a 16-fold degeneracy.[17] The solutions are reduced to 4 if one considers the regular patterns of the dipolar couplings (i.e., dipolar waves) in secondary structures.[8,18−22] In favorable cases, this inherent degeneracy is resolved using two or more alignment media.[23] Nonetheless, local geometry can still be ill-defined[17] and further confounded by the presence of conformational dynamics.[24−27] Therefore, a major issue is to eliminate ghost orientations from the true orientations. To this extent, Bertini and co-workers have proposed the use of paramagnetic-based NMR restraints.[28] These authors have developed a new analysis of PREs to give a comprehensive view of the different conformations and dynamics of calmodulin as well as the calmodulin−α-synuclein complex.[28] A similar approach has been utilized for resolving the solution conformation of the ternary complex of the *E. coli* Hsp70 chaperone.[29]

Membrane proteins solubilized in detergent micelles are not immune to these challenges. Polytopic membrane proteins are often organized in multiple domains (independent or partially independent) that facilitate intra- and intercellular communication.[30] Membrane protein tertiary structures are often defined by domain interactions with the lipid membrane, that is, topology.[31] Several small and medium size membrane proteins involved in regulatory function of ion pumps fall into this category.[31] While membrane proteins are amenable to modern solution NMR techniques, it is still a challenging task to obtain long-range distance restraints from NOE data,[32] especially for helical membrane proteins. Side-chain methyl labeling schemes can help determine the overall fold of membrane proteins, and new protocols have been developed to introduce a variety of different probes.[33−36] RDCs constitute a viable alternative to obtaining long-range distance restraints for membrane proteins. To measure RDCs, membrane proteins need to be aligned in an anisotropic medium[37−39] or bound to a lanthanide ion through adventitious sites[40] or engineered tags.[41,42] In several instances, RDCs were crucial for

Received: October 22, 2010
Published: February 2, 2011

improving the resolution of membrane protein structures solubilized in micelles.[32,43,44]

In this Article, we show that the ghost orientations generated after RDC refinement of the detergent-solubilized protein phospholamban (PLN) can be eliminated by using paramagnetic-based restraints derived from site-directed spin-labeling using MTSSL (1-oxyl-2,2,5,5-tetramethyl-D3-pyrroline-3-methyl methanethiosulfonate).

MATERIALS AND METHODS

PLN Expression, Purification, and Mutagenesis. The overexpression and purification of AFA−PLN (i.e., cysteine-null monomer, C36A, C41F, C46A) was carried out as described in Buck et al.[45] For the A24C mutant, the plasmid encoding cysteine-null PLN was used as a template to introduce a single point mutation (A24C) by site directed mutagenesis using a Quick-change kit (Stratagene, San Diego, CA). The primers were designed as follows: forward 5′-GCCGCAGCAGTGCCGCCAGAACCTGC-3′, reverse 5′-GCAGGTCTGGCGGCACTGCTGCGGC-3′ (the mutated codon is underlined). The steps of the PCR protocol were reported previously.[45]

The mutated plasmid was amplified in XL1-blue competent cells (Stratagene, San Diego, CA) and purified using QIAprep Spin kit (Qiagen, Carlsbad, CA). The sequence was confirmed by DNA sequencing (ABI PRISM 3130xl Genetic Analyzer, Biomedical Genomic Center, Minneapolis, MN). BL21(DE3) (Stratagene, San Diego, CA) *E. coli* cells were transformed with 100 ng of purified plasmid and selected on LB agar plates containing ampicillin (100 mg/mL). The L7C and R9C mutants were designed in a similar way. Protein expression and purification were carried out using a combination of affinity chromatography and HPLC. The steps of the PCR protocol were reported previously.[45]

A24C−AFA−PLN and L7C−AFA−PLN Spin-Labeling with MTSSL. The spin labeling reaction protocol was optimized by Kirby et al.[46] One milligram of lyophilized A24C−AFA−PLN (or L7C−AFA−PLN) protein was solubilized in 1 mL of spin labeling buffer (60 mM Tris−HCl at pH 7.0 and 0.2% SDS). The final concentration of PLN was ∼0.2 mM. A 10-fold molar excess of MTSSL (1-oxyl-2,2,5,5-tetramethyl-D3-pyrroline-3-methyl methanethiosulfonate, Toronto Research Chemicals, North York, ON) was added to the reaction mix and incubated overnight at 4 °C in the dark. The unreacted spin label was removed by reversed-phase HPLC. Lyophilized MTSSL spin-labeled A24C−AFA−PLN (or L7C−AFA−PLN) was dissolved in 300 mM DPC, 20 mM phosphate buffer (pH = 6.0), 120 mM NaCl, 0.01% NaN_3, and 10% D_2O. The final concentrations of A24C−AFA−PLN and L7C−AFA−PLN were ∼0.1 mM. Labeling efficiency was measured by EPR.[46]

Sample Preparation for RDC Measurements. AFA−PLN [U−^{13}C, ^{15}N] was reconstituted into 100 mM deuterated DPC (Cambridge Isotope Laboratories), 25 mM phosphate buffer (pH 6.0), 120 mM NaCl, 10% D_2O, and 0.1% NaN_3 to give a final protein concentration of ∼0.8 mM. The stretched gels were polymerized from a 5.7 mm diameter cylinder under the following conditions: 100 mM Tris−HCl (pH 8.0), 5.1% acrylamide, 1.3% bis-acrylamide, 0.1% ammonium persulfate, and 0.33% TEMED. The gels were washed twice with 50 mM NaH_2PO_4/Na_2HPO_4 pH 6.5 (8 h/wash) and then twice with H_2O (8 h/wash) as described previously.[47] The protein/detergent mixture was added to the dried polymerized gel and incubated at 37 °C for ∼24 h. After being stretched in a 5 mm Shigemi tube, the length of the gel increased by a factor of ∼1.7. The stretching apparatus was purchased from New Era Enterprises, Inc.[47]

NMR Spectroscopy. *RDC Measurements.* NMR experiments were carried out at 37 °C using a Varian spectrometer operating at a ^{1}H Larmor frequency of 599.54 MHz. 2D TROSY-based (^{1}H, ^{15}N) pulse sequences described by Permi and Annila[48] were used to measure

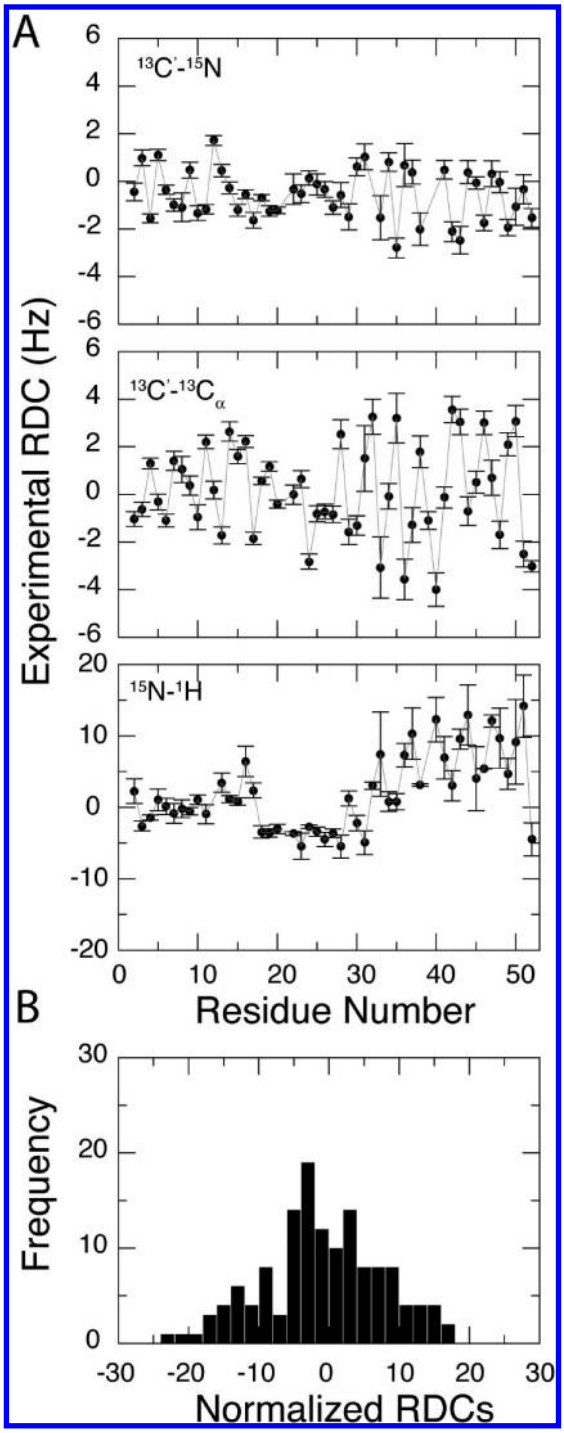

Figure 1. RDCs versus residue for AFA−PLN weakly oriented in stretched gels. (A) Top, $^{13}C'_{i-1}-^{15}N_i$ RDCs; middle, $^{13}C'-^{13}C_\alpha$ RDCs; bottom, $^{15}N-^1H$ RDCs. We reported only the RDC values for well-resolved peaks. (B) RDC histogram with all the data in (A) scaled to the $^{15}N-^1H$ RDCs.

$^{13}C'-^{15}N$ and $^{15}N-^1H$ one-bond *J*-couplings (and *J*-coupling + RDC). Each 2D experiment was acquired in the presence and absence of the stretched gel, where the difference in splitting allowed for the calculation of the RDCs. The total acquisition times in t_1 and t_2 were 62 and 77 ms with spectral widths of 1300 and 6600 Hz in the ^{15}N and ^{1}H dimensions, respectively. To measure the $^{13}C'-^{13}C_\alpha$ one-bond couplings, we performed a 3D uncoupled HNCO experiment in the presence and

dx.doi.org/10.1021/ja109080t |*J. Am. Chem. Soc.* 2011, 133, 2232–2241

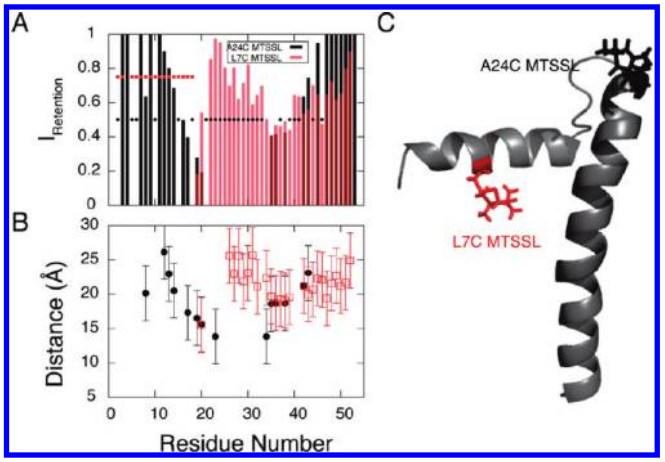

Figure 2. PRE data obtained from A24C−AFA−PLN (black) and L7C−AFA−PLN (red) cross-linked with MTSSL. (A) Intensity retention plot for A24C−AFA−PLN and L7C−AFA−PLN labeled with MTSSL. Unresolved peaks or completely quenched peaks are marked with asterisks. (B) Distances derived from PREs (see Materials and Methods). Only peaks with an intensity retention ratio less than 0.95 were used in the calculations. Also, some residues lacking R_2 values were omitted. (C) Cartoon representation of PLN with the MTSSL label at C24 and C7.

absence of stretched gel. Experiments were performed with 64 scans, spectral widths of 10 000 Hz (^{1}H), 1000 Hz (^{13}C), and 1200 Hz (^{15}N), and total acquisition times of 83.2, 40, and 26.7 ms in the ^{1}H, ^{13}C, and ^{15}N dimensions, respectively. A recycle delay of 1.3 s was used for all of the experiments. All data were processed with NMRPipe[49] and analyzed using NMRVIEW.[50] The ^{15}N−^{1}H, ^{13}C′−^{15}N, and ^{13}C′−^{13}C$_\alpha$ RDCs versus residue are shown in Figure 1A.

PRE Measurements. [^{1}H, ^{15}N] heteronuclear single quantum coherence (HSQC) spectra were acquired in the presence of MTSSL (paramagnetic) and the diamagnetic analogue at positions 7 and 24 of PLN. The intensity reductions of the amide resonances were converted into R_2^{sp} values and then to distance restraints using eq 1:[51]

$$\frac{I_{ox}}{I_{red}} = \frac{R_2\, e^{-R_2^{sp} t}}{R_2 + R_2^{sp}}$$

$$r = \left[\frac{K}{R_2^{sp}}\left(4\tau_c + \frac{3\tau_c}{1+\omega_{H^2}\tau_c^2}\right)\right]^{1/6} \quad (1)$$

where I_{ox} and I_{red} are the peak intensities corresponding to the oxidized and reduced MTSSL samples, respectively, r is the distance between the nuclear spins and the unpaired electron, τ_c is the correlation time for the electron/nuclear spin interaction, ω_H is the proton Larmor frequency, R_2 and R_2^{sp} are the transverse relaxation rates in the absence and presence of spin label, respectively, and K is a constant (1.23×10^{-32} cm^6 s^{-2})that depends on the gyromagnetic ratio, electronic g factor, and the Bohr magneton.

For PLN, we used two different correlation times (τ_c): 8.2 ns for the cytoplasmic domain and 15.4 ns for the transmembrane domain.[52] For peaks with intensity retention greater than 90% no upper limit distances were used. For the other peaks, the intensity retentions were converted into distances according to eq 1 and implemented with upper and lower limit distances of ±4 Å.[51] The PRE data and the calculated distance restraints for PLN are shown in Figure 2.

Calculation Protocol. We used the standard energy target function implemented in XPLOR-NIH:[53]

$$E = E_{empirical} + E_{solution} \quad (2)$$

where $E_{empirical}$ is the sum of the energy terms for the covalent geometry (bond distance, bond angles, improper angles) and VDW interactions:

$$E_{empirical} = w_{bonds}E_{bonds} + w_{angles}E_{angles} + w_{impropers}E_{impropers} + w_{vdw}E_{vdw} \quad (3)$$

$E_{solution}$ includes the penalty functions for distance and orientational restraints (NOEs, dihedral angles, RDCs, and PREs):

$$E_{solution} = w_{NOE}E_{NOE} + w_{CDIH}E_{CDIH} + w_{DB}E_{DB} + w_{RDC}E_{RDC} + w_{PRE}E_{PRE} \quad (4)$$

All of the NOE-derived distance restraints used in the present study were taken from the previously published structure of PLN in DPC micelles.[54] A total of 373 distances (142 intra-residue and 231 inter-residue) were included. In addition, 58 hydrogen bonds derived from H/D exchange measurements were used. Finally, we obtained 38 dihedral angle restraints using the program TALOS[55] based on the chemical shifts of H$_\alpha$, C$_\alpha$, C$_\beta$, C′, N, and H$_N$.[56] All of the restraints used in the calculations are listed in Table S1.

To illustrate the impact of RDC and PRE restraints in the structural refinement of PLN, three simulated annealing protocols were used to generate three different structural ensembles.[57] In the first protocol, the restraints derived from typical solution NMR experiments, including NOE-derived distances, dihedral angle restraints and hydrogen bonds were used.[54] The second protocol included the restraints from the first protocol plus RDCs derived from the partial alignment of PLN in stretched gels. Finally, the third protocol was constructed by adding MTSSL distance restraints determined from PRE data to all constraints used in the first two protocols. Details for the calculation are presented in the Supporting Information.

RESULTS

Structural Refinement with NOE and Dihedral Angle Restraints (Protocol One). To test our approach, we used phospholamban (PLN), a 52-residue integral membrane protein in the sarcoplasmic reticulum (SR) that regulates the SR Ca^{2+}-ATPase (SERCA).[58] PLN exists as a pentamer in the SR and depolymerizes to monomers upon encountering SERCA.[59,60] To induce the monomeric state, we mutated the three transmembrane Cys residues (C36A, C41F, C46A) to obtain a stable monomer with activity identical to that of wild-type PLN.[61] The NMR structure of PLN monomer in dodecylphosphocholine micelles has been solved by our group.[54] For the structure determination, we used distance restraints derived from ^{15}N-edited NOESY spectra, dihedral restraints from chemical shifts,[55] and hydrogen bonds from H/D exchange factors.[62] On the basis of the calculations and subsequent backbone dynamics studies, we identified four dynamic domains: α-helical domain Ia (residues 1−16), α-helical region spanning domains Ib (residues 23−30) and II (residues 31−52), and a loop connecting the two helical regions (residues 17−22).[52]

Given the limited amount of distance and angular restraints found between the loop and its adjacent domains, the final structural ensemble resulted in many different conformers with poor convergence for the overall backbone conformation and topology. In our previous paper,[54] we mapped solvent accessibility using Mn^{2+} ions and the insertion of PLN in the micelles using 5- and 16-DSA (doxyl stearic acids), and we manually eliminated structures that contradicted the paramagnetic mapping. We concluded that PLN adopts a helical L-shaped conformation with the cytoplasmic

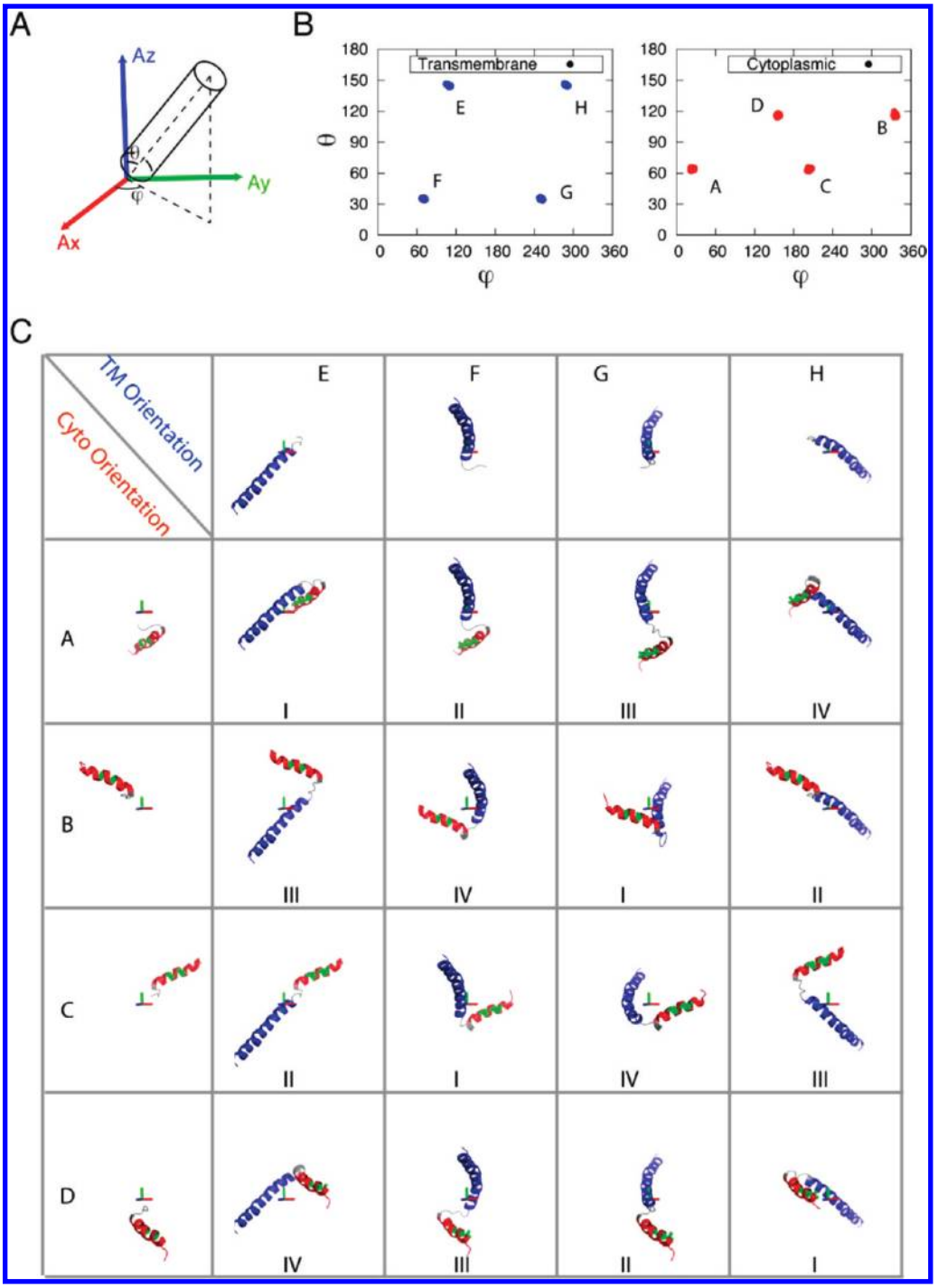

Figure 3. (A) Definition of orientation angles θ and φ for a rigid body helix in the alignment frame. (B) θ and φ plots for the cytoplasmic (Cyto, red) and transmembrane (TM, blue) domain orientations in the alignment frame. (C) Orientation of TM and Cyto domains with each letter corresponding to the θ and φ angles defined in (B). Different combinations of orientations result in different families (labeled in the bottom as I, II, III, and IV). The green color on the cytoplasmic domain indicates hydrophobic residues.

amphipathic domain Ia adsorbed on the surface of the micelle. These results were also supported by solid-state NMR experiments carried out in lipid bilayers.[63] While these studies represent the initial characterization of PLN in membrane mimicking environments, they were limited by two factors: (a) the absence of topological restraints (the selection of conformers was carried out manually), and (b) the absence of the relative orientation of the two helical domains.

Structural Refinement with RDCs and NOEs (Protocol Two). To improve the solution NMR structural ensemble of PLN, we introduced restraints from three sets of RDCs obtained from the partial alignment of PLN in a stretched gel system.[37,64] Figure 1 shows the three sets of RDCs used in the calculations. As expected from the helical secondary structure of PLN, the values of the RDCs oscillate periodically. There is a significant change in the pattern from residues 20 to 30 for the $^{15}N-^{1}H$ RDCs.

dx.doi.org/10.1021/ja109080t |J. Am. Chem. Soc. 2011, 133, 2232–2241

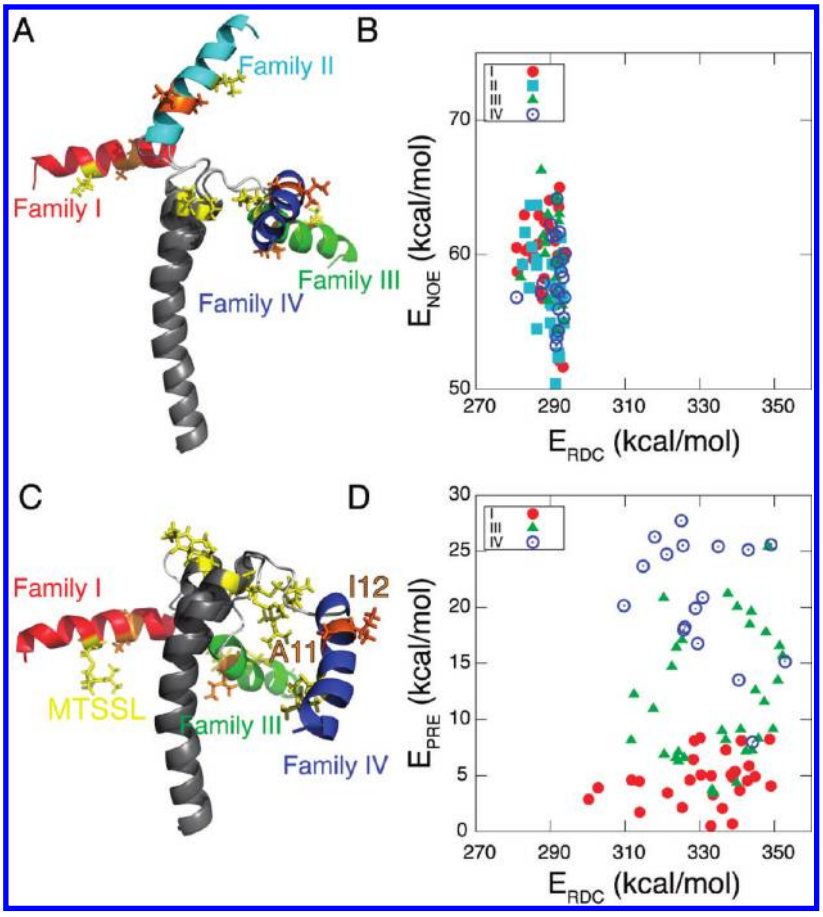

Figure 4. (A) Comparison between representative structures from each family refined with protocol two. Side chains of the MTSSL spin label (yellow) and hydrophobic residues (A11 and I12, orange) are shown and labeled. (B) E_{NOE} and E_{RDC} of the four families of structures from protocol two. (C). Similar to (A) except for protocol three. (D) E_{PRE} and E_{RDC} of the three families of structures from protocol three.

These residues belong to domain Ib, a helical region that is more dynamic and solvent exposed than the transmembrane domain II.[52] When fitting these dynamically averaged RDCs to an average structure, a pronounced kink is observed between domain Ib and domain II. CPMG relaxation dispersion measurements obtained from PLN in DPC indicate the presence of chemical exchange (at least two conformations) for domain Ib,[52,65] and for this reason we excluded RDCs from domain Ib during our structural calculation. Dynamic model or ensemble simulations are needed to explain the discontinuity of the RDC pattern in this domain.

One of the challenges for structural refinement with RDCs is to accurately determine the axial (D_a) and rhombic (R) components of the alignment tensor. Several methods are available to estimate these values such as the maximum likelihood method by Moore and Warren[66] and the histogram method by Bax and coworkers.[67] To use these methods, large numbers of RDCs are needed, and their reliability is dependent on the accuracy of the experimental measurements. Because of the increased size of membrane proteins within detergent micelles, experimental RDCs have larger errors than their soluble counterparts. Furthermore, the errors for $^{13}C'-^{15}N$ and $^{13}C'-^{13}C_\alpha$ RDCs are much larger after scaling to those of the $^{15}N-^{1}H$ RDCs. To overcome this, D_a and R were allowed to vary in the simulated annealing procedure.[6] This introduced two extra parameters into the structural fitting in addition to the tensor orientations. Four hundred structures were generated and clustered based on two groups of D_a and R values (Figure S1). The solutions with $D_a = -8$ Hz and $R = 0.667$ resulted in poor fitting of the RDCs. These structures were excluded from further analysis. The structures generated from the second group (shown red in Figure 3) with $D_a = 8.6$ (± 0.3) and $R = 0.52$ (± 0.04) were used in the following calculations. The high rhombicity R is consistent with the RDC histogram shown in Figure 1B. Note that all of the RDCs were implemented in the simulated annealing protocol using a flat-well potential.[53]

The force constants for RDCs during the structure refinement were determined using the R factor method (R_{RDC}) as described by Clore and co-workers.[57] Two variables were monitored as a function of the RDC force constant: (1) the R factor for different sets of RDCs and (2) the penalties from energy terms other than RDCs. During the force constant ramping, the tensor values D_a and R were fixed (determined above to be $D_a = 8.6$ and $R = 0.52$). The best value for the force constant was 0.5 kcal mol^{-1} Hz^{-2} (see Figure S1), which gives reasonable RDC agreement without large penalties from other structural and experimental restraints.

After optimizing D_a, R, and the force constants, we generated ~300 structures and selected the 100 lowest energy structures for further analysis (Figure 4A,B). The resulting structures were clustered into four distinct families (Figure 5B). These structures differ in the relative orientation of the two helical domains, giving rise to a 4-fold degeneracy (Figure 5B). Each structural ensemble shows a backbone rmsd less than 1.6 Å, with good correlations

dx.doi.org/10.1021/ja109080t | J. Am. Chem. Soc. 2011, 133, 2232–2241

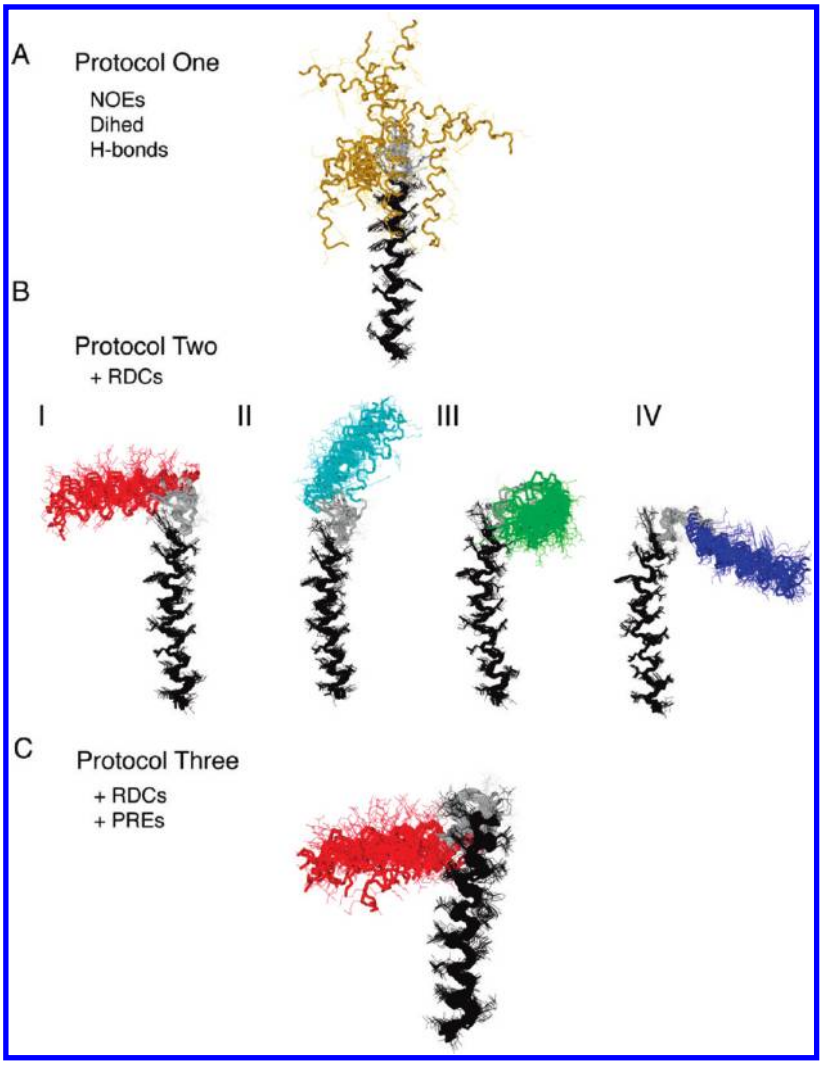

Figure 5. Overlay of different AFA-PLN conformational ensembles obtained by superimposing backbone atoms from residues 24−50 using MOLMOL. (A) Protocol one: ensemble obtained from NOEs, torsion angles, and hydrogen bonds (20 monomers). (B) Protocol two: RDC ensemble (15 monomers) with $^{15}N-^{1}H$, $^{13}C'-^{15}N$, and $^{13}C'-^{13}C_{\alpha}$ RDCs. (C) Protocol three: PRE ensemble (20 monomers) that utilizes PREs from MTSSL in addition to the restraints used in protocol two.

between experimental and calculated RDC values (Figures S2). When viewed in the alignment tensor frame (Figure 3C), 16 different solutions for two helical domain structures are possible. A similar result has been obtained by Bax and co-workers[68] for the monomeric subunit of KcsA solubilized in detergent micelles.

The solutions can be distinguished by analyzing the orientation angles (θ, φ) for each helical domain in the alignment tensor frame (Figure 3) as well as the interhelical angle χ (angle between domains Ia and II, red and blue, respectively). The orientations correspond to the following angles: (θ, φ), $(\theta, \pi+\varphi)$, $(\pi-\theta, \pi-\varphi)$, and $(\pi-\theta, 2\pi-\varphi)$ (Figure 3B). The degenerate solutions agree with theoretical equations describing RDC periodicity.[20,21,22] The hydrophobic residues of the cytoplasmic domain Ia are oriented toward the transmembrane domain for families I and II and away from it for families III and IV (Figure 5A). Family I has a χ angle of ∼90°, while families III and IV display χ angles of ∼70°. Family II has a nearly antiparallel orientation between the two helical domains (χ∼140°). This orientation is similar to that obtained by Oxenoid and Chou.[69]

Structural Refinement with NOEs, RDCs, and PREs (Protocol Three). To reduce the degeneracy from the RDC solutions and remove the translational degree of freedom between the two domains, we implemented PRE distance restraints from two MTSSL−PLN constructs (L7C−AFA−PLN and A24C−AFA−PLN). These restraints were included in the calculations using the convention introduced by Battiste and Wagner[51](see Materials and Methods). To restrict the flexibility of the spin label, we used a dihedral angle potential (sinusoid potential) for the χ_1, χ_2, and χ_3 angles of the spin label, which adopt defined values as determined from the crystal structures.[70]

In protocol two (RDC+NOE refinement), the four families are energetically degenerate (E_{RDC} and E_{NOE}) (Figure 4A,B), while in protocol three, these three families have different values of E_{PRE} (Figure 4C,D). The structures within family I display the lowest PRE and NOE energies and thus were selected as the final ensemble (Figure 5C), with a backbone rmsd of ∼1.2 Å and good agreement with experimental RDCs (Figures S4) and PREs (Figure S5).

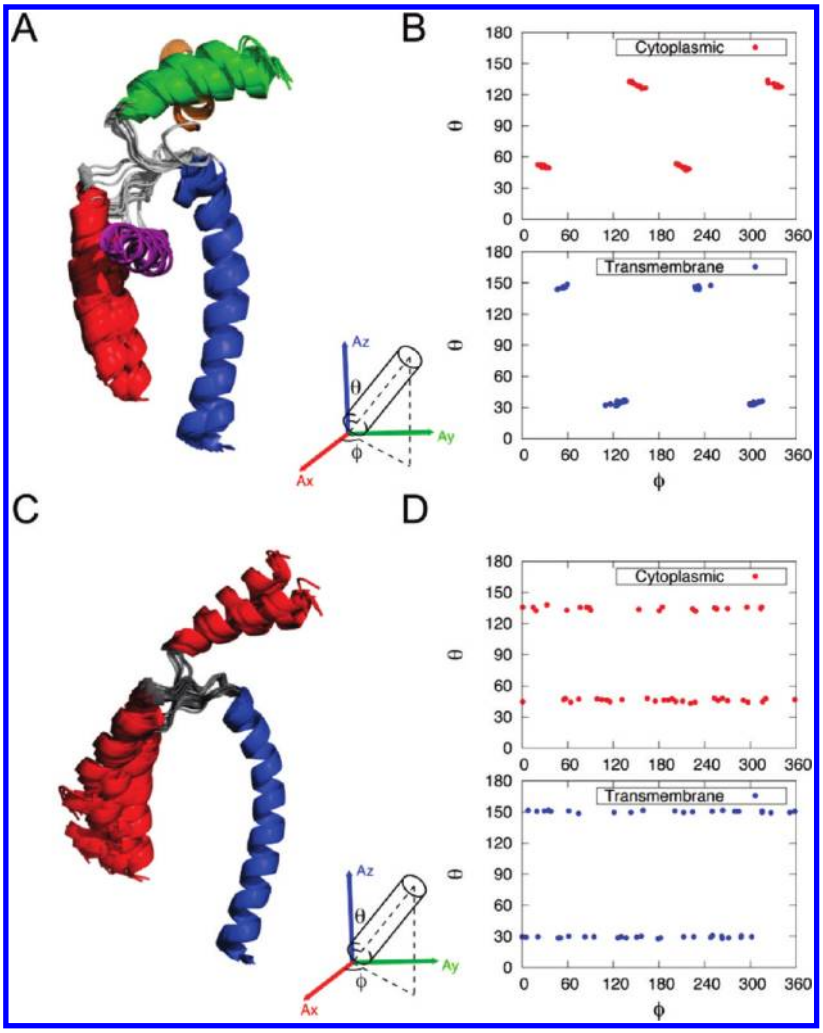

Figure 6. (A) Overlay of monomer structures calculated using wt-PLN RDCs[69] with an asymmetric tensor ($R \neq 0$). (B) Orientation angles (θ, φ) of helical rigid bodies in the asymmetric alignment frame ($R \neq 0$). (C) Overlay of monomer structures calculated using wt-PLN RDCs[69] with a symmetric tensor ($R = 0$). (D) Orientation angles (θ, φ) of helical rigid bodies in the symmetric alignment frame ($R = 0$).

The energy differences between families I, III, and IV are very small and cannot be used as a criterion for selection. However, only family I has the hydrophobic residues facing toward the transmembrane helix, that is, facing the micelle interior (Figure 4C). As an attempt to further support our selection criteria to eliminate families III and IV, we labeled PLN with MTSSL at position 9 (R9C−PLN). When the MTSSL is engineered, the long chain of MTSSL cross-linked to Cys 9 inserts in the detergent micelle (see quenching of the resonances in the transmembrane domain in Figure S6C), resulting in an incorrect positioning of the side chain and faulty interpretation of the structural topology of the protein. Therefore, the flexibility and hydrophobic nature of the MTSSL spin label calls for special care when engineering site-specific mutants in membrane proteins when those sites are proximal to the membrane.[71]

RDC Analysis for the PLN Pentamer. The structure of the PLN pentamer heavily relied on the use of RDCs in the structure refinement.[69] In fact, the structure of individual monomers were built prior to assembly the symmetric pentamer. In the calculation of the monomeric units, the alignment tensors (D_a = 9.00, R = 0.33) were determined from singular value decomposition (SVD)[72] using $^{15}N-^{1}H$, $^{13}C-^{15}N$, and $^{13}C'-^{13}C_\alpha$ RDCs. The alignment tensor was slightly different from the value we obtained for monomeric AFA-PLN. A comparison of RDC restraints between the pentamer (Oxenoid and Chou[69]) and monomer (this Article) showed a good correlation (Figure S7), especially with the $^{15}N-^{1}H$ RDCs. We then performed a similar structural calculation using Oxenoid and Chou's data.[69] We obtained four degenerate solutions (Figure 6A,B) as for the AFA−PLN monomer. On the basis of these results, we speculate that the authors[69] selected one of the solutions from the structural ensembles to build the pentamer.

Aside from the degeneracy issue, the choice of the tensor value for a symmetric pentamer is also debatable. It is well-known[15] that for oligomeric proteins the symmetry axis should coincide with the long axes of the alignment tensor, resulting in $R = 0$ (zero rhombicity). It was argued that asymmetric tensor values could result from protein dynamics;[69] however, the dynamic averaging of RDCs needs to be interpreted using a dynamic ensemble rather than fitting data to an average structure. We also refined the monomeric unit using RDCs measured by Oxenoid and Chou[69] with a symmetric tensor ($R = 0$). The D_a value obtained was 6.5, using the methods described earlier (Figure S1). Figures 6C and D show that the ϕ angles do not have defined

dx.doi.org/10.1021/ja109080t |J. Am. Chem. Soc. 2011, 133, 2232–2241

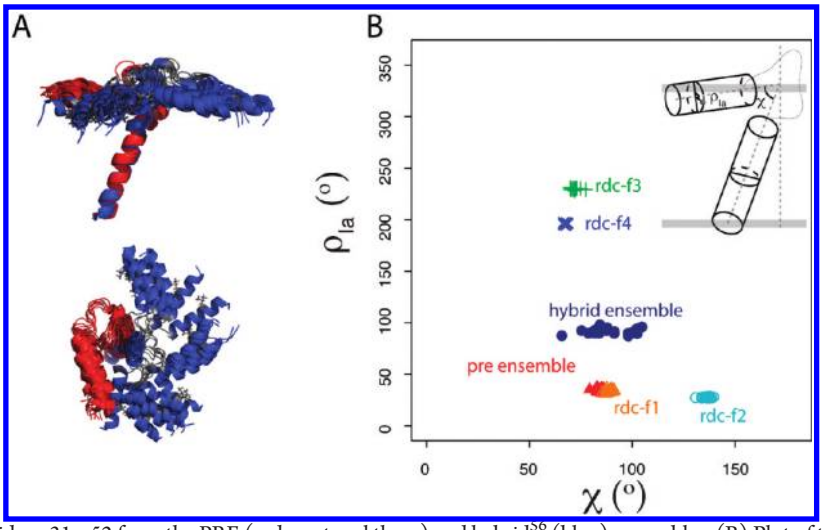

Figure 7. (A) Overlay of residues 31−52 from the PRE (red, protocol three) and hybrid[56] (blue) ensembles. (B) Plot of the interhelical angle (χ) with the rotation angle of domain Ia (ρ) from the RDC-degenerate families (f1, orange; f2, cyan; f3, green; and f4, blue), PRE ensemble from protocol three (red), and hybrid ensemble (blue). The definitions of the χ and ρ angles are shown within panel B.

minima. This is also in agreement with a theoretical study, which showed that an infinite number of solutions exist for $R = 0$.[17]

DISCUSSION

To address the challenges of high-resolution structure determination of membrane proteins in micelles, the classical NOE-driven approach has been supplemented with RDCs. However, internal protein dynamics and intrinsic degeneracy of the RDC solutions complicate the data interpretation, resulting in ghost orientations. Here, we show that the degeneracy problem can be addressed by including RDC restraints with PREs from covalent attachment of the MTSSL spin label, which provides a fast and efficient method for determination of both membrane protein structure and topology.

We applied this method to a small multidomain membrane protein, PLN, which regulates the enzymatic activity of the SR Ca^{2+}-ATPase in cardiac muscle. While structural biologists agree on the secondary structure content of the transmembrane domain of PLN, there is an active debate about the topological arrangement of this protein in the lipid membrane.[58] The structure calculations carried out with NOE-based distance restraints do not provide a high-resolution picture of PLN due to the lack of restraints between the helical domains. In our original work, the correct orientations of the helical domains of PLN were selected manually based on the PRE data from Mn^{2+} and doxyl stearic acids.[54] The introduction of RDCs improves the resolution of the ensemble, but exemplifies four degenerate solutions, with ghost orientations of the cytoplasmic domain Ia. The combination of paramagnetic-based restraints with RDCs and NOEs enabled us to resolve the orientation that agrees best with all available data. This solution (family I) is similar to the recently determined structural ensemble of monomeric PLN in lipids.[56,73] This is not surprising because several recent reports have shown that the structures of membrane proteins in micelles are similar to those determined in lipid bilayers.[74] The slight discrepancy in the average rotation angles between the hybrid ensemble and that determined by combining NOEs, RDCs, and PREs (Figure 7) has several possible origins. First, there are approximations in estimating the alignment tensor. Second, the cytoplasmic domain of PLN is rather dynamic,[52,65] and our interpretation of RDCs and PREs[76] does not take this into account. Third, the nonplanar surface of the micelle can cause bends and curvature to malleable domains of membrane proteins and peptides.[47,75] Fourth, RDCs provide information of bond orientations with respect to three alignment tensor axes in an asymmetric tensor. Orientational data from PISEMA experiments in oriented samples[56] only encode bond orientations with respect to one of the tensor axis (z axis), similar to RDCs with a symmetric tensor.

Because the studies of membrane proteins in detergent micelles are likely to continue to offer insightful information, we conclude that for multidomain membrane proteins the use of RDCs is not sufficient to define their conformational space and topology. Rather, orientational restraints need to be supplemented with long-range paramagnetic restraints from spin labels covalently linked to proteins to uniquely define their topology.[32,77]

Finally, we would like to point out that this Article addresses only the geometric ambiguities derived from RDCs. In fact, intrinsic dynamics complicates the interpretation of both PREs and RDCs for structure determination. To overcome these problems, molecular dynamics methods are being developed for the variability of alignment tensors[78,79] as well as for the modulations of the PRE effects on long-range interactions.[76,80] A more comprehensive approach for flexible domains of membrane proteins will require the combined use of PREs and RDCs using ensemble molecular dynamics methods.[76]

ASSOCIATED CONTENT

Supporting Information. Additional figures of alignment tensor (Da,R) clustering, RDC R factors, RDC correlations for RDC-generated families, RDC correlation for the PRE ensemble, PRE correlations for the PRE ensemble, PREs for R9C-MTSSL labeled PLN, RDC correlation between monomer and pentamer PLN, and a table with structural statistics from different refinement protocols. This material is available free of charge via the Internet at http://pubs.acs.org.

AUTHOR INFORMATION

Corresponding Author
vegli001@umn.edu

■ ACKNOWLEDGMENT

This work was supported by grants to G.V. from the National Institutes of Health (GM64742, HL80081) and the American Heart Association (0160465). L.S. was supported by a Doctoral Dissertation Fellowship from the University of Minnesota graduate school. This work was carried out in part using hardware and/or software provided by the University of Minnesota Supercomputing Institute.

■ REFERENCES

(1) Tjandra, N.; Bax, A. *Science* **1997**, *278*, 1111–1114.
(2) Bax, A.; Kontaxis, G.; Tjandra, N. *Methods Enzymol.* **2001**, *339*, 127–174.
(3) Prestegard, J. H. *Nat. Struct. Biol.* **1998**, 517.
(4) Prestegard, J. H.; Al-Hashimi, H. M.; Tolman, J. R. *Q. Rev. Biophys.* **2000**, *33*, 371–424.
(5) Tjandra, N.; Marquardt, J.; Clore, M. G. *J. Magn. Reson.* **2000**, *142*, 393–396.
(6) Clore, M. G.; Gronenborn, M. A.; Tjandra, N. *J. Magn. Reson.* **1998**, *131*, 159–162.
(7) Nodet, G.; Salmon, L.; Ozenne, V.; Meier, S.; Jensen, M. R.; Blackledge, M. *J. Am. Chem. Soc.* **2009**, *131*, 17908–17918.
(8) Jensen, M. R.; Blackledge, M. *J. Am. Chem. Soc.* **2008**, *130*, 11266–11267.
(9) Meier, S.; Blackledge, M.; Grzesiek, S. *J. Chem. Phys.* **2008**, *128*, 052204.
(10) Jha, A. K.; Colubri, A.; Freed, K. F.; Sosnick, T. R. *Proc. Natl. Acad. Sci. U.S.A.* **2005**, *102*, 13099–13104.
(11) Marsh, J. A.; Forman-Kay, J. D. *J. Mol. Biol.* **2009**, *391*, 359–374.
(12) Vallurupalli, P.; Hansen, D. F.; Stollar, E.; Meirovitch, E.; Kay, L. E. *Proc. Natl. Acad. Sci. U.S.A.* **2007**, *104*, 18473–18477.
(13) Baldwin, A. J.; Hansen, D. F.; Vallurupalli, P.; Kay, L. E. *J. Am. Chem. Soc.* **2009**, *131*, 11939–11948.
(14) Fischer, M. W. F.; Losonczi, J. A.; Weaver, J. L.; Prestegard, J. H. *Biochemistry* **1999**, *38*, 9013–9022.
(15) Al-Hashimi, H. M.; Bolon, P. J.; Prestegard, J. H. *J. Magn. Reson.* **2000**, *142*, 153–158.
(16) Mueller, G. A.; Choy, W. Y.; Yang, D.; Forman-Kay, J. D.; Venters, R. A.; Kay, L. E. *J. Mol. Biol.* **2000**, *300*, 197–212.
(17) Hus, J. C.; Salmon, L.; Bouvignies, G.; Lotze, J.; Blackledge, M.; Bruschweiler, R. *J. Am. Chem. Soc.* **2008**, *130*, 15927–15937.
(18) Mesleh, M. F.; Veglia, G.; DeSilva, T. M.; Marassi, F. M.; Opella, S. J. *J. Am. Chem. Soc.* **2002**, *124*, 4206–4207.
(19) Mesleh, M. F.; Opella, S. J. *J. Magn. Reson.* **2003**, *163*, 288–299.
(20) Mascioni, A.; Veglia, G. *J. Am. Chem. Soc.* **2003**, *125*, 12520–12526.
(21) Walsh, J. D.; Wang, Y. X. *J. Magn. Reson.* **2005**, *174*, 152–162.
(22) Mascioni, A.; Eggimann, B. L.; Veglia, G. *Chem. Phys. Lipids* **2004**, *132*, 133–144.
(23) Al-Hashimi, H. M.; Valafar, H.; Terrell, M.; Zartler, E. R.; Eidsness, M. K.; Prestegard, J. H. *J. Magn. Reson.* **2000**, *143*, 402–406.
(24) Tolman, J. R.; Flanagan, J. M.; Kennedy, M. A.; Prestegard, J. H. *Proc. Natl. Acad. Sci. U.S.A.* **1995**, *92*, 9279–9283.
(25) Tolman, J. R.; Flanagan, J. M.; Kennedy, M. A.; Prestegard, J. H. *Nat. Struct. Biol.* **1997**, *4*, 292–7.
(26) Tolman, J. R.; Ruan, K. *Chem. Rev.* **2006**, *106*, 1720–1736.
(27) Lakomek, N. A.; Carlomagno, T.; Becker, S.; Griesinger, C.; Meiler, J. *J. Biomol. NMR* **2006**, *34*, 101–115.
(28) Bertini, I.; Gupta, Y. K.; Luchinat, C.; Parigi, G.; Peana, M.; Sgheri, L.; Yuan, J. *J. Am. Chem. Soc.* **2007**, *129*, 12786–12794.
(29) Bertelsen, E. B.; Chang, L.; Gestwicki, J. E.; Zuiderweg, E. R. *Proc. Natl. Acad. Sci. U.S.A.* **2009**, *106*, 8471–8476.
(30) White, S. H.; Wimley, W. C. *Annu. Rev. Biophys. Biomol. Struct.* **1999**, *28*, 319–365.
(31) von Heijne, G. *Nat. Rev. Mol. Cell Biol.* **2006**, *7*, 909–918.
(32) Zhou, Y.; Cierpicki, T.; Jimenez, R. H.; Lukasik, S. M.; Ellena, J. F.; Cafiso, D. S.; Kadokura, H.; Beckwith, J.; Bushweller, J. H. *Mol. Cell* **2008**, *31*, 896–908.
(33) Traaseth, N. J.; Verardi, R.; Veglia, G. *J. Am. Chem. Soc.* **2008**, *130*, 2400–2401.
(34) Tugarinov, V.; Kay, L. E. *J. Biomol. NMR* **2004**, *28*, 165–72.
(35) Tugarinov, V.; Kay, L. E. *J. Am. Chem. Soc.* **2003**, *125*, 13868–13878.
(36) Gross, J. D.; Gelev, V. M.; Wagner, G. *J. Biomol. NMR* 2003, *25*, 235–242.
(37) Tycko, R.; Blanco, F. J.; Ishii, Y. *J. Am. Chem. Soc.* **2000**, *122*, 9340–9341.
(38) Douglas, S. M.; Chou, J. J.; Shih, W. M. *Proc. Natl. Acad. Sci. U.S. A.* **2007**, *104*, 6644–6648.
(39) Lorieau, J.; Yao, L.; Bax, A. *J. Am. Chem. Soc.* **2008**, *130*, 7536–7537.
(40) Veglia, G.; Opella, S. J. *J. Am. Chem. Soc.* **2000**, *122*, 11733–11734.
(41) Ma, C.; Opella, S. J. *J. Magn. Reson.* **2000**, *146*, 381–384.
(42) Wohnert, J.; Franz, K. J.; Nitz, M.; Imperiali, B.; Schwalbe, H. *J. Am. Chem. Soc.* **2003**, *125*, 13338–13339.
(43) Van Horn, W. D.; Kim, H. J.; Ellis, C. D.; Hadziselimovic, A.; Sulistijo, E. S.; Karra, M. D.; Tian, C.; Sonnichsen, F. D.; Sanders, C. R. *Science* **2009**, *324*, 1726–1729.
(44) Cierpicki, T.; Liang, B.; Tamm, L. K.; Bushweller, J. H. *J. Am. Chem. Soc.* **2006**, *128*, 6947–6951.
(45) Buck, B.; Zamoon, J.; Kirby, T. L.; DeSilva, T. M.; Karim, C.; Thomas, D.; Veglia, G. *Protein Expression Purif.* **2003**, *30*, 253–61.
(46) Kirby, T. L.; Karim, C. B.; Thomas, D. D. *Biochemistry* **2004**, *43*, 5842–52.
(47) Chou, J. J.; Kaufman, J. D.; Stahl, S. J.; Wingfield, P. T.; Bax, A. *J. Am. Chem. Soc.* **2002**, *124*, 2450–2451.
(48) Permi, P.; Annila, A. *J. Biomol. NMR* **2000**, *16*, 221–227.
(49) Delaglio, F.; Grzesiek, S.; Vuister, G. W.; Zhu, G.; Pfeifer, J.; Bax, A. *J. Biomol. NMR* **1995**, *6*, 277–293.
(50) Johnson, B. A. *Methods Mol. Biol.* **2004**, *278*, 313–352.
(51) Battiste, J. L.; Wagner, G. *Biochemistry* **2000**, *39*, 5355–5365.
(52) Metcalfe, E. E.; Zamoon, J.; Thomas, D. D.; Veglia, G. *Biophys. J.* **2004**, *87*, 1205–1214.
(53) Schwieters, C. D.; Kuszewski, J. J.; Tjandra, N.; Clore, G. M. *J. Magn. Reson.* **2003**, *160*, 65–73.
(54) Zamoon, J.; Mascioni, A.; Thomas, D. D.; Veglia, G. *Biophys. J.* **2003**, *85*, 2589–2598.
(55) Cornilescu, G.; Delaglio, F.; Bax, A. *J. Biomol. NMR* **1999**, *13*, 289–302.
(56) Traaseth, N. J.; Shi, L.; Verardi, R.; Mullen, D. G.; Barany, G.; Veglia, G. *Proc. Natl. Acad. Sci. U.S.A.* **2009**, *106*, 10165–10170.
(57) Clore, G. M.; Kuszewski, J. *J. Am. Chem. Soc.* **2003**, *125*, 1518–1525.
(58) Traaseth, N. J.; Ha, K. N.; Verardi, R.; Shi, L.; Buffy, J. J.; Masterson, L. R.; Veglia, G. *Biochemistry* **2008**, *47*, 3–13.
(59) Kimura, Y.; Kurzydlowski, K.; Tada, M.; MacLennan, D. H. *J. Biol. Chem.* **1997**, *272*, 15061–4.
(60) Reddy, L. G.; Jones, L. R.; Thomas, D. D. *Biochemistry* **1999**, *38*, 3954–62.
(61) Karim, C. B.; Marquardt, C. G.; Stamm, J. D.; Barany, G.; Thomas, D. D. *Biochemistry* **2000**, *39*, 10892–7.
(62) Veglia, G.; Zeri, A. C.; Ma, C.; Opella, S. J. *Biophys. J.* **2002**, *82*, 2176–2183.
(63) Mascioni, A.; Karim, C.; Zamoon, J.; Thomas, D. D.; Veglia, G. *J. Am. Chem. Soc.* **2002**, *124*, 9392–9393.
(64) Chou, J. J.; Gaemers, S.; Howder, B.; Louis, J. M.; Bax, A. *J. Biomol. NMR* **2001**, *21*, 377–382.
(65) Traaseth, N. J.; Veglia, G. *Biochim. Biophys. Acta* **2010**, *1798*, 77–81.
(66) Warren, J. J.; Moore, P. B. *J. Magn. Reson.* **2001**, *149*, 271–275.
(67) Clore, M. G.; Gronenborn, M. A.; Bax, A. *J. Magn. Reson.* **1998**, *133*, 216–221.

(68) Chill, J. H.; Louis, J. M.; Delaglio, F.; Bax, A. *Biochim. Biophys. Acta* **2007**, *1768*, 3260–3270.
(69) Oxenoid, K.; Chou, J. J. *Proc. Natl. Acad. Sci. U.S.A.* **2005**, *102*, 10870–10875.
(70) Langen, R.; Oh, K. J.; Cascio, D.; Hubbell, W. L. *Biochemistry* **2000**, *39*, 8396–8405.
(71) Sammalkorpi, M.; Lazaridis, T. *Biophys. J.* **2007**, *92*, 10–22.
(72) Losonczi, J. A.; Andrec, M.; Fischer, M. W.; Prestegard, J. H. *J. Magn. Reson.* **1999**, *138*, 334–342.
(73) Shi, L.; Traaseth, N. J.; Verardi, R.; Cembran, A.; Gao, J.; Veglia, G. *J. Biomol. NMR* **2009**, *44*, 195–205.
(74) Franzin, C. M.; Teriete, P.; Marassi, F. M. *J. Am. Chem. Soc.* **2007**, *129*, 8078–8079.
(75) Chou, J. J.; Kaufman, J. D.; Stahl, S. J.; Wingfield, P. T.; Bax, A. *J. Am. Chem. Soc.* **2002**, *124*, 2450–2451.
(76) Dedmon, M. M.; Lindorff-Larsen, K.; Christodoulou, J.; Vendruscolo, M.; Dobson, C. M. *J. Am. Chem. Soc.* **2005**, *127*, 476–477.
(77) Liang, B.; Bushweller, J. H.; Tamm, L. K. *J. Am. Chem. Soc.* **2006**, *128*, 4389–4397.
(78) Salvatella, X.; Richter, B.; Vendruscolo, M. *J. Biomol. NMR* **2008**, *40*, 71–81.
(79) De Simone, A.; Richter, B.; Salvatella, X.; Vendruscolo, M. *J. Am. Chem. Soc.* **2009**, *131*, 3810–3811.
(80) Salmon, L.; Nodet, G.; Ozenne, V.; Yin, G.; Jensen, M. R.; Zweckstetter, M.; Blackledge, M. *J. Am. Chem. Soc.* **2010**, *132*, 8407–8418.